Statistics of quiet Sun extreme ultraviolet intensities

A. Pauluhn[1,2]**, S.K. Solanki**[3]**, I. Rüedi**[4]**, E. Landi**[3]**, and U. Schühle**[3]

[1] INTEC HTA Bern, Switzerland
[2] Institut of Astronomy, ETH Zürich, Switzerland
[3] Max-Planck-Institut für Aeronomie, Katlenburg-Lindau, Germany
[4] Physikalisch Meteorologisches Observatorium, World Radiation Center Davos, Switzerland

Abstract. The frequency distribution of the extreme ultraviolet (EUV) emission line intensities in the quiet Sun has in the past often been modelled using two Gaussians. This gives adequate fits to observed distributions of average statistical significance. In this paper we test this and other distribution functions against observed distributions with exceptional statistical significance. The data were obtained in a number of spectral lines observed with two extreme ultraviolet spectrometers on board the Solar and Heliospheric Observatory (SOHO). In this way, the influence of spatial resolution and other instrument-specific parameters can be identified. The observations span a period of more than two years and provide a very large data set of radiance measurements of the quiet Sun at or near solar disk centre. We show that the frequency distribution of the radiance is best modelled by a lognormal distribution. The fact that the radiance distribution of the quiet Sun including the network and the intranetwork is better reproduced by a *single* lognormal distribution function than by two Gaussians suggests that the same heating processes are acting in both types of features.

The parameters of the lognormal fit show a clear temperature dependence, with the transition region lines exhibiting the largest skewness of the distribution and the chromospheric intensity distributions being the most symmetric.

Key words: Sun: UV radiation – Sun: chromosphere – Sun: transition region – Sun: corona

1. Introduction

The extreme ultraviolet (EUV) emission of the quiet Sun forms a pattern of brighter and darker structures. The bright parts (referred to as the chromospheric or transition region network) surround darker cells with a diameter of approximately 30000 km. The brightness enhancements in the network result from concentrations of magnetic field, which in turn are produced by convection in the photospheric supergranules (e.g. Leighton 1959; Martin 1988). Several models describe the extension of the magnetic field from small areas between the cells of the photospheric supergranules into broad structures in the corona (Gabriel 1976; Athay 1982; Dowdy et al. 1986; Solanki & Steiner 1990).

Intensity distributions of the quiet Sun have been investigated in older studies (Huber et al. 1974; Reeves 1976; Reeves et al. 1976) based on Skylab data and more recently using data from the Solar Ultraviolet Measurements of Emitted Radiation (SUMER) instrument (Lemaire et al. 1997; Bocchialini et al. 1997; Griffiths et al. 1999; Dammasch et al. 1999) and the Coronal Diagnostic Spectrometer (CDS) (Gallagher et al. 1998). All studies show that the quiet Sun radiance follows a distribution with a pronounced peak and a long tail extending to high intensities. The skewed form of the distribution precludes a fit with a single Gaussian. Reeves (1976) decomposed the radiance distribution obtained with Skylab data into a sum of two Gaussian distributions, which he interpreted as describing the network and the cell radiance. Gallagher et al. (1998) carried out a similar decomposition of CDS data. Griffiths et al. (1999) investigated SUMER observations of the quiet Sun transition region and found that the emission line intensities are consistent with a lognormal distribution. Which of these approaches - double Gaussian or lognormal - provides a better description can only be decided on the basis of a large amount of data, i.e. distributions of extremely high statistical significance. Distinguishing between a one-component (lognormal) and a two-component (double Gaussian) description is of potential interest, since it gives a hint on whether chromospheric and coronal heating distinguishes between network and cell interiors or not.

In this paper we contribute to the statistical description of the quiet Sun in several ways. Firstly, by discussing and testing various possible models for the frequency distribution of the radiances. Secondly, we compare distributions obtained with two different instruments, SUMER and CDS onboard SOHO (Solar and Heliospheric Observatory). Thirdly, our statistics are based on more than two years (March 1996 to June 1998) of almost monthly observations and thus should give a representative sample of quiet Sun radiances. The extremely good statistics needed in order to distinguish between different functional representations of the distributions are thus achieved. Finally, we consider normalized distributions, which allows us to follow the change in the shape of the distribution as a function of formation temperature of the emitting ions.

Send offprint requests to: A. Pauluhn (pauluhn@astro.phys.ethz.ch)

In the following (Sect. 2) we briefly describe the CDS and SUMER observational data. Sect. 3 gives the frequency distributions in the various wavelengths and their fits. In Sect. 4 we search for a relation between temperature and the parameters of the distribution function, and in Sect. 5 the results are summarized.

2. Observational data

SUMER (Wilhelm et al. 1995) observes in the wavelength range from 465 to 1610 Å, depending on the spectral order and the choice of detector. Its spectral resolution is 44 mÅ/pixel in first order and 22 mÅ/pixel in second order and its spatial resolution is 1″. The CDS (Harrison et al. 1995) normal incidence spectrometer (NIS) observes in the two bands from 310 to 380 Å and from 517 to 633 Å. The spectral pixel size of the CDS NIS ranges from 0.070 Å at 310 Å to 0.118 Å at 630 Å. The effective pixel size of CDS is 4″ in horizontal (cross slit) direction and 1.68″ vertical (along slit), although the actual spatial resolution is lower (Thompson 1998; Haugan 1999). Since the beginning of the SOHO mission an intercalibration programme has been carried out which includes simultaneous observations of CDS and SUMER of common targets near solar disk centre devoid of any notable activity (Pauluhn et al. 1999). The spectral lines recorded simultaneously during these measurements were He I at 584 Å and the two Mg X lines at 609 Å and 624 Å. SUMER additionally observed in Ne VIII 770 Å and since September 1996 also in N V 1238 Å. Our sample of lines with good statistics thus covers formation temperatures ranging from 2×10^4 K to 1×10^6 K, i.e. the chromosphere, transition region and corona.

Each measurement consisted of a raster scan over an extended area with a spectrum recorded at every spatial position. The instruments scanned an area of $60'' \times 240''$ (CDS), and $60'' \times 300''$ (SUMER, prior to November 1996). After SUMER's scanning mechanism was disabled, the SUMER spectrometer slit was kept fixed, and the scanning was produced by solar rotation during the exposure time, limiting the raster size to about 4″ in the cross-slit direction.

The SUMER data were corrected for the flatfield, for the geometric image distortion, and the electronic dead-time of the detector. The CDS data were corrected for burn-in and the flatfield. After the instrumental corrections and the radiometric calibration, the solar radiances were determined by integration over the line profiles, which were derived by least-squares fits of single or multi-Gaussian functions and a linear background. For more information on the data and the reduction we refer to Pauluhn et al. (1999).

3. Intensity statistics of the quiet Sun

Although the radiances of the two instruments agree well within their uncertainties (Pauluhn et al. 1999), CDS measures on average 30% higher radiance values than SUMER in the He I line (for the data analyzed here). For the Mg X 609 Å and 624 Å lines this difference is 17% and 9%, respectively. The important point is, however, that both instruments exhibit the same long-term temporal trends, suggesting that fluctuations from one scan to the next are solar, which allows us to combine the various observations to form histograms with extremely high S/N. It has to be noted that the 609 Å line is blended with an O IV line formed at a temperature of $T = 2 \times 10^5$ K with a lower region of formation than the corona (Thompson & Brekke 1999), and thus its histograms do not represent a "pure" coronal line like those of the 624 Å line.

The intensities of each spectral line and of each instrument have been binned before forming histograms. The binsize has been chosen such as to provide a high enough resolution, but also to be larger than the instrumental noise. The resulting binsizes are 0.05 W/m²/sr for He I, 0.005 for Mg X 609 Å, 0.001 for Mg X 624 Å, and 0.003 for N V and Ne VIII.

We tested five statistical models of probability functions against the data: a Rayleigh distribution, a Maxwellian distribution, a superposition of two Gaussian distributions, a lognormal distribution, and a superposition of a lognormal and a Gaussian distribution.

The Rayleigh and Maxwell distributions are positively skewed functions defined on a positive data range. In the following μ and σ denote the mean and the standard deviation, respectively, and x is the intensity.

Rayleigh:

$$\rho(x) = \frac{N_0 x}{c^2} e^{-\frac{x^2}{2c^2}}, \quad x \geq 0, \qquad c = \sqrt{\frac{2}{\pi}}\,\mu \tag{1}$$

Maxwell:

$$\rho(x) = \frac{N_0 x^2}{c^3} e^{-\frac{x^2}{2c^2}}, \quad x \geq 0, \qquad c = \sqrt{\frac{\pi}{2}}\frac{\mu}{2} \tag{2}$$

Double Gaussian:

$$\rho(x) = N_1 e^{-\frac{(x-\mu_1)^2}{2\sigma_1^2}} + N_2 e^{-\frac{(x-\mu_2)^2}{2\sigma_2^2}} \tag{3}$$

Lognormal:

$$\rho(x) = \frac{N_0}{x} e^{-\frac{(\ln(x)-\mu)^2}{2\sigma^2}} \tag{4}$$

Lognormal+Gaussian:

$$\rho(x) = \frac{N_1}{x} e^{-\frac{(\ln(x)-\mu_1)^2}{2\sigma_1^2}} + N_2 e^{-\frac{(x-\mu_2)^2}{2\sigma_2^2}} \tag{5}$$

The lognormal distribution is strongly peaked and positively skewed and well suited to model a frequency distribution with a sharp maximum and a pronounced tail. The Maxwellian and Rayleigh distributions have the advantage of the fewest free fit parameters (2 for unnormalized, 1 for normalized frequency distributions, where "normalized" means divided by the number of pixels). The lognormal has 3 and 2 free parameters, respectively. Finally, the double Gaussian fit and lognormal plus Gaussian combinations involve 6 free parameters for unnormalized distributions and 5 for normalized ones. Fits consisting of two distributions introduce a natural distinction between brighter and darker parts of the solar atmosphere, usually equated with
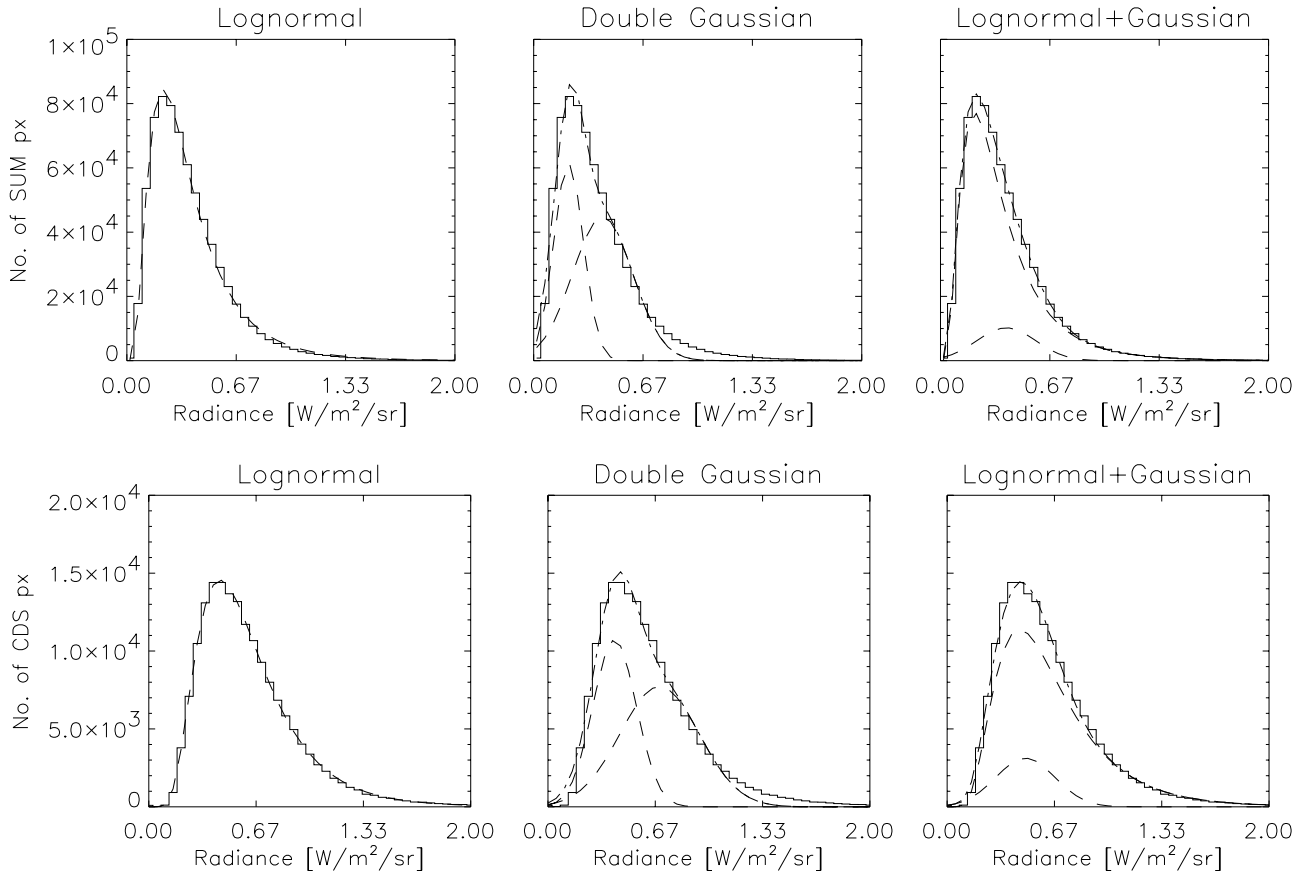
Fig. 1. Upper row: SUMER frequencies of occurrence at He I 584 Å, fitted with the 3 different models. Lower row: The same for the CDS frequencies of occurrence.

the network and cell interiors, while a single distribution suggests that there is no principle distinction between various parts of the quiet Sun, at least not a simple one.

The lognormal, double Gaussian and lognormal+Gaussian fits to the observed distributions are plotted in Figs. 1–4. Fig. 1 shows the results for the He I 584 Å line ($T = 2 \times 10^4$ K). In the upper row the SUMER data and corresponding fits are plotted, while the lower row shows the same for the CDS data. Figs. 2 and 3 show the same but for the coronal lines Mg X 609 Å and Mg X 624 Å ($T = 1 \times 10^6$ K). The fits based on the Maxwell and Rayleigh distribution functions are not plotted due to their relatively poor quality.

In Fig. 4 the results for the transition region lines N V 1238 Å ($T = 1.7 \times 10^5$ K; upper panels) and Ne VIII 770 Å ($T = 6 \times 10^5$ K; lower panels) are shown (SUMER data only).

The χ^2-differences are given in Table 1, where we computed χ^2 as the sum over the squared differences between the normalized observed and functional distributions.

Table 2 gives the fractions of the intensities that are represented by the fits and, in the case of the 2-component fits, of the individual components, respectively (the latter given in brackets). Finally, Fig. 5 depicts the discrepancies between the fits and the data. As an example we present the results for the Ne VIII 770 Å line, as observed by SUMER. In Fig. 5a the absolute difference is plotted, $f_i - F_i$, while in Fig. 5b the asymmetry,

$\frac{f_i - F_i}{f_i + F_i}$, is shown, where F denotes the model distribution and f the data. The latter is a measure of the relative difference between fit and data. It is obvious that the Rayleigh and Maxwell distributions are not suitable to model the quiet Sun data. Also, the two Gaussians are somewhat better at representing the height of the maximum, whereas the tails can only be reproduced by a lognormal. It is clear from this figure that the Rayleigh and Maxwell distributions are far inferior to the rest in the quality of the fit produced. This is confirmed by Table 1.

A careful study of Figs. 1–5 and Tables 1 and 2 reveals the following:

1) The double Gaussian fit (6 free parameters) captures more than 80% of the intensity and seems to be a reasonable approximation over the main body of the distribution. It is, however, unable to account for the prominent tail of the distributions, in spite of the large number of free parameters.

2) The lognormal distribution (3 free parameters) alone covers more than or nearly 90% of the intensity in all temperature ranges. The errors in reproducing the original data intensities vary from 2–12%. The lognormal distribution is able to represent the tails of the distributions quite accurately. It provides an almost perfect fit for the transition region and chromospheric lines, with a steady decrease in quality towards higher temperatures.
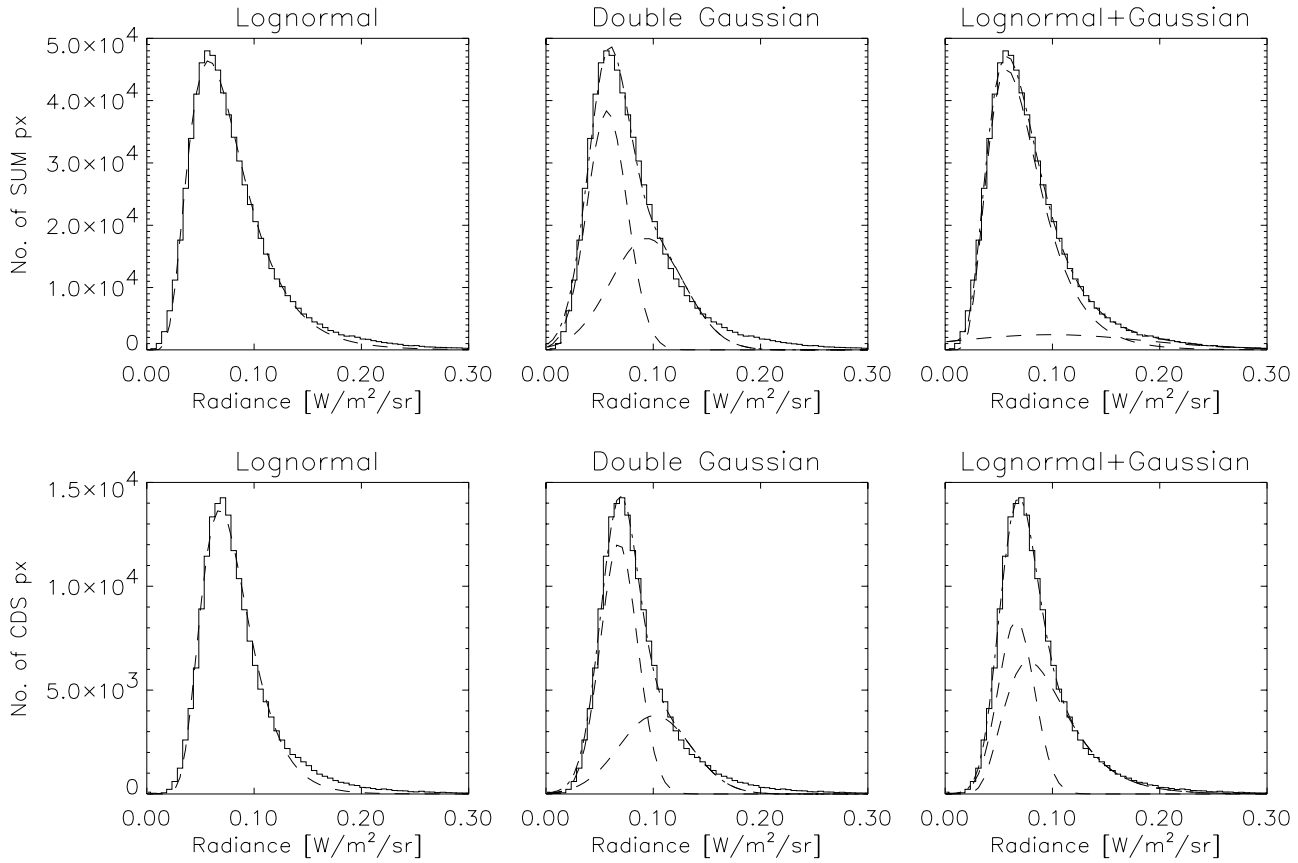
Fig. 2. Upper row: SUMER frequencies of occurrence at Mg X 609 Å, fitted with the 3 different models. Lower row: The same for the CDS frequencies of occurrence. (Note that this line contains a strong blend of a lower temperature line (O IV, $T = 2 \times 10^5$ K).

Table 1. Error of the fits (χ^2-differences).

	584 Å		1238 Å		770 Å		609 Å		624 Å	
	CDS	SUMER	CDS	SUMER	CDS	SUMER	CDS	SUMER	CDS	SUMER
Rayleigh	5.0×10^{-3}	5.7×10^{-3}	–	3.7×10^{-3}	–	1.3×10^{-3}	1.1×10^{-2}	4.6×10^{-3}	4.4×10^{-3}	2.1×10^{-3}
Maxwell	4.1×10^{-3}	1.3×10^{-2}	–	7.8×10^{-3}	–	1.5×10^{-3}	6.5×10^{-3}	3.8×10^{-3}	2.6×10^{-3}	2.7×10^{-3}
2 G	3.6×10^{-4}	5.7×10^{-4}	–	2.7×10^{-4}	–	1.5×10^{-4}	1.2×10^{-4}	1.9×10^{-4}	1.1×10^{-4}	7.9×10^{-5}
logn	1.2×10^{-5}	1.0×10^{-4}	–	2.5×10^{-5}	–	1.2×10^{-4}	2.3×10^{-4}	7.8×10^{-5}	1.8×10^{-4}	6.6×10^{-5}
logn+G	1.8×10^{-5}	1.4×10^{-5}	–	1.1×10^{-5}	–	4.1×10^{-6}	2.6×10^{-5}	2.5×10^{-5}	4.5×10^{-5}	1.2×10^{-5}

Table 2. Fractions of the radiance contained in the components of the fits.

	584 Å		1238 Å		770 Å		609 Å		624 Å	
	CDS	SUMER	CDS	SUMER	CDS	SUMER	CDS	SUMER	CDS	SUMER
2 G	87.8 (27.4,60.4)	84.4 (21.5,62.9)	–	71.8 (17.0,54.8)	–	90.7 (26.6,64.1)	91.1 (47.9,43.2)	87.5 (36.3, 51.2)	90.1 (43.0,47.1)	84.5 (35.9, 48.6)
logn	98.5	101.8	–	97.6	–	101.7	87.4	92.2	87.5	91.1
logn+G	98.1 (12.8,85.3)	99.6 (13.4,86.1)	–	95.6 (3.7,91.1)	–	99.8 (23.8,76.0)	95.3 (31.5,63.8)	98.6 (19.9,78.7)	93.9 (35.3, 58.6)	96.0 (17.0, 79.0)

3) The combined model of a lognormal and a Gaussian (6 free parameters) provides the best fit to the quiet Sun intensity data distributions for most lines, in particular those formed at coronal temperatures. It reproduces the original distributions to within 0.5–6%. In the colder lines the Gaussian gives less than a 15% contribution to the total, while for the coronal lines - especially for the CDS measurements - the Gaussian represents a large frac-

tion of the total intensity. However, the gain in precision over the single lognormal fit is only achieved at the price of doubling the number of free parameters. Also, the lognormal+Gaussian combination suffers from the fact that the contribution of the Gaussian component differs by up to a factor of 2 between SUMER and CDS data (Table 2), although this may be due to the different spatial resolutions of the two instruments. More serious
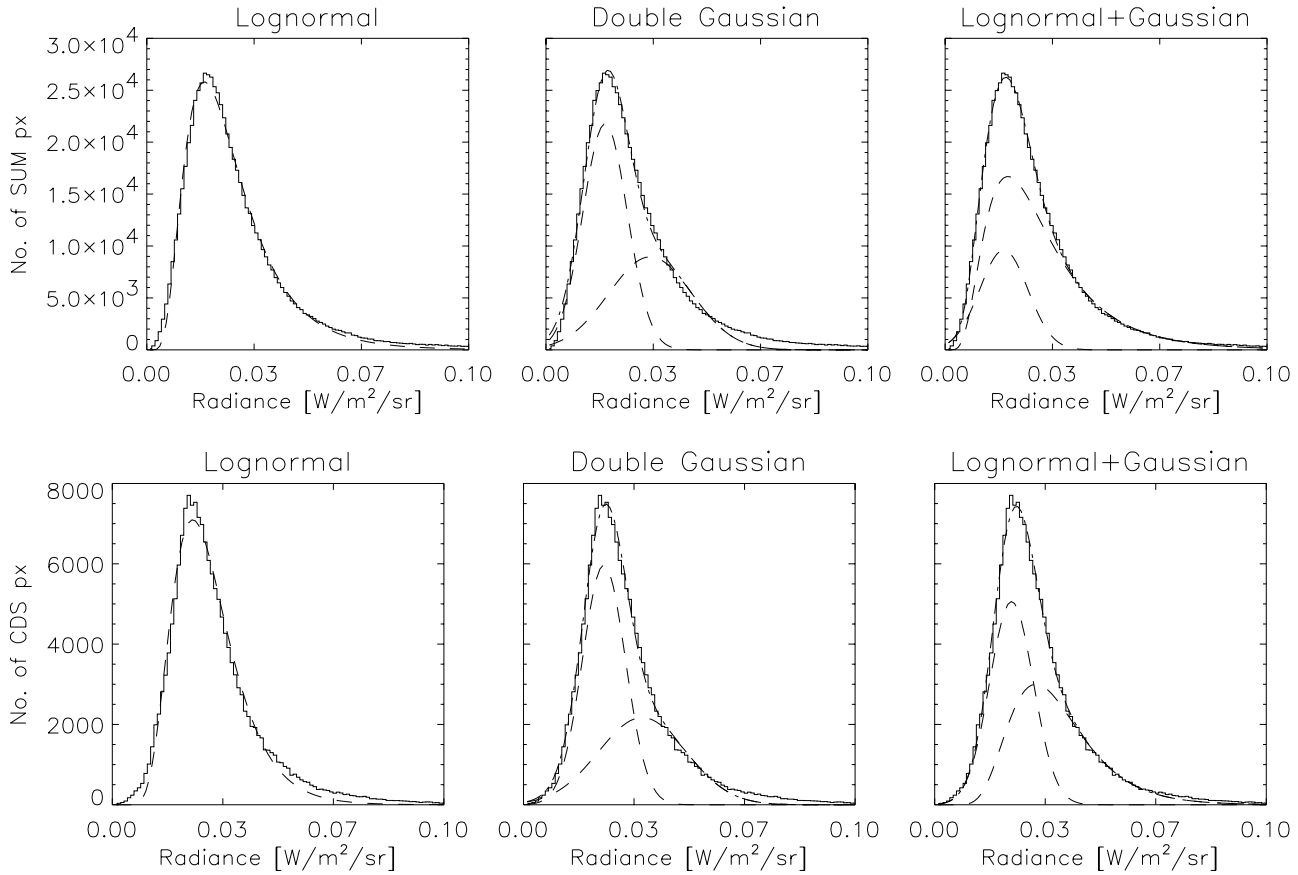
Fig. 3. Upper row: SUMER frequencies of occurrence at Mg X 624 Å, fitted with the 3 different models. Lower row: The same for the CDS frequencies of occurrence.

is that, unlike in the case of the double Gaussian, the relative strengths and locations of the two components vary strongly from fit to fit. This suggests that the distinction between the two components is arbitrary and not particularly stable, so that the improvement of some of the fits is mainly a consequence of the increased number of free parameters.

It is interesting that for the coronal lines, i.e. those with the poorest lognormal fits, the lognormal+Gaussian fits are significantly better for the SUMER than for the CDS data. We checked whether this is due to the difference in spatial resolution between the two instruments by degrading the SUMER data obtained with detector A, where raster scans over an area of $60'' \times 300''$ had been made, to the CDS resolution. They were smoothed by a suitable point-spread-function and rebinned to the CDS spatial pixel size as described by Pauluhn et al. (1999). The histograms of all data of these 7 rasters in He I and 6 rasters in Mg X were then fitted using the Gaussian and lognormal functions. In general the errors of the fits increased relative to those found for the undegraded data. The fact that both Mg X lines measured by CDS are better represented by the sum of two Gaussians than by a single lognormal also turns out to be a result of the poorer spatial resolution of CDS, since the degraded SUMER data exhibit the same effect. Finally, the lower resolution of the degraded SUMER data lead to a change in the partition of intensity contents in the 2-component models for He I 584 Å and Mg X 609 Å: the lower intensity ("cells" in the case of the two Gaussians) Gaussian component then contained approximately half of the total intensity. This also agrees with the findings from fits to CDS and SUMER (see Table 2). This shows that the main differences between the histograms obtained from SUMER and CDS scans are due to the difference in spatial resolution between the two instruments. However, only for the lines formed at higher temperature do the distributions change with resolution, for the chromospheric He I 584 Å line there was no improvement at higher resolution. It therefore seems that the spatial elements contributing to the EUV emissions of lower temperature regions can be resolved, whereas for coronal lines the available SUMER resolution is not sufficient, and the size of these heating elements lies at or below SUMER's resolution of $1''$.

4. Temperature dependence of the distribution function

To study the dependence of the parameters of the distributions we included more data in the chromospheric and transition region temperature ranges. The additional data sets in the range between $10^{4.0}$ K and $10^{4.35}$ K were SUMER raster scans covering $60'' \times 120''$ made in Jun. 1996 in the lines C I 1311 Å and C II 1334 Å, and a time series in the O I line at 1152 Å made in
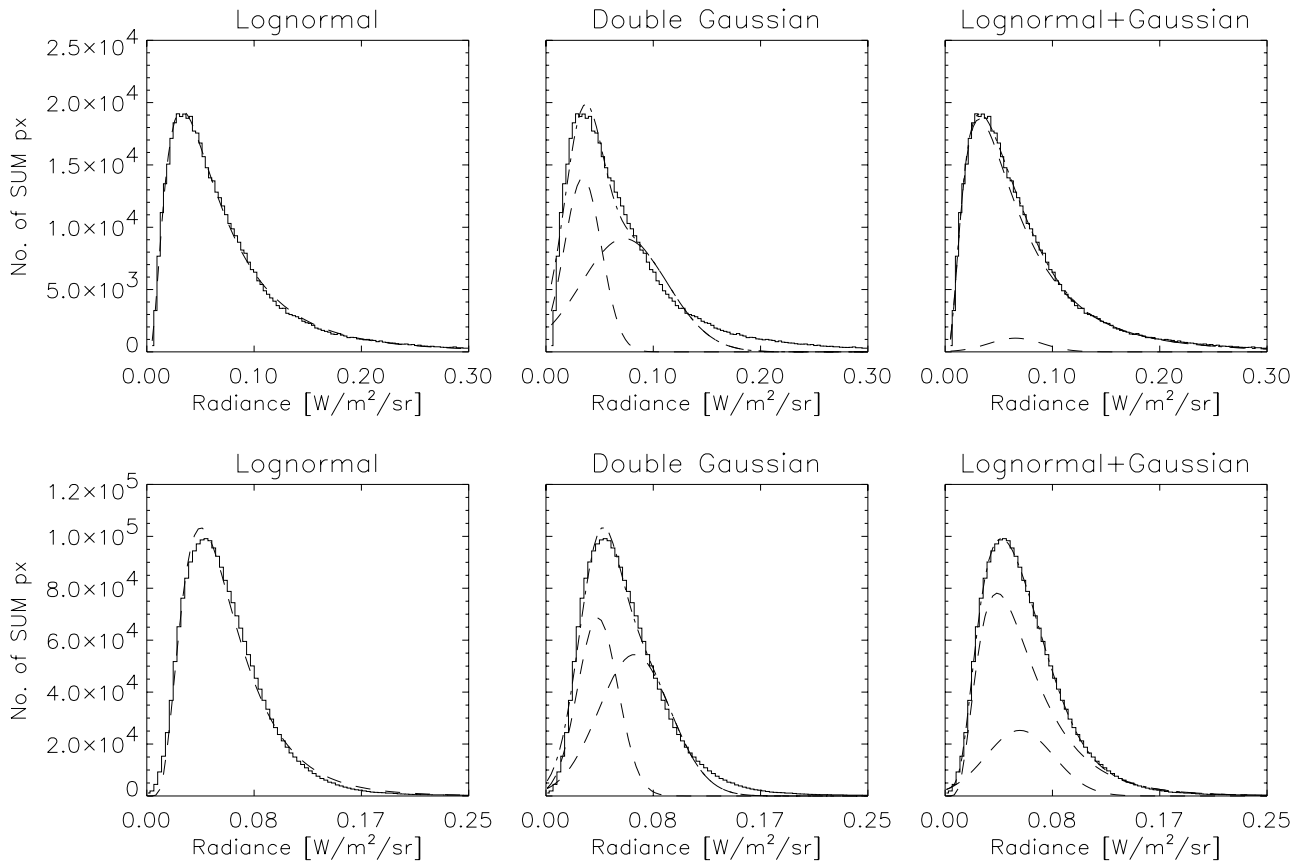
Fig. 4. Upper row: SUMER frequencies of occurrence at N V 1238 Å, fitted with the 3 different models. Lower row: The same for the Ne VIII 770 Å line.

Mar. 1996. In the range between $10^{4.5}$ K and $10^{5.5}$ K SUMER raster scans covering $90'' \times 100''$ were available, made in Sept. 1996 in the lines Si IV 1402 Å, O III 703 Å, O IV 1401 Å, and O V 629 Å. A lognormal fit was made to all distributions. We normalized the shape of the fitted distributions with respect to the number of pixels and additionally rescaled the radiance to a common range by dividing by the mean value.

Fig. 6a shows the fitted lognormal distribution functions of all available data in the temperature range between 10^4 K and 10^6 K. The transition region lines show significantly different distribution shapes. These lines have their most common value in a lower radiance regime but their tails extend further out than for the chromospheric and coronal lines indicating that there is a greater probability for relatively high radiance values. This could be due to the large number of short-time scale enhancements seen at these temperatures. The chromospheric lines have a sharper peak at higher radiances, and their tails drop off more steeply. Finally, the coronal lines exhibit an intermediate behaviour. Fig. 6b depicts one of the corresponding fit parameters, namely the strength (N_0 from Eq. (4)), which measures the height and position of the most probable radiance value. The larger this parameter, the higher the peak and the more "outward" shifted and symmetric is the shape of the lognormal function. This figure qualifies the results already visible in Fig. 6a.

Figs. 7a and b show the corresponding position (μ) and width (σ) parameters of the fitted lognormal functions. As pointed out by J. G. Doyle (priv. communication) the shape of the curve in Fig. 7b looks similar to that of the Doppler shifts versus temperature profile found by a number of authors (e.g. Teriaca et al. 1999 and references therein). The chromospheric lines showing little or no Doppler shift have the most symmetric and "peaked" radiance distributions, the transition region lines with pronounced redshifts exhibit large tails in their radiance distributions. It is, however, unclear to what extent or how these two results are related.

5. Discussion and conclusions

We have tested several statistical representations of a large data set of quiet Sun measurements in chromospheric, transition region and coronal lines. The observations have been performed by the EUV spectrometers CDS and SUMER over a period of more than two years including the end of solar activity cycle 22 and the beginning of cycle 23.

The radiance distributions of the quiet Sun observations of both instruments can be almost optimally modelled by a lognormal distribution or with even slightly better accuracy by a combination of a lognormal and a Gaussian distribution. A double Gauss model, although having the advantage of separating
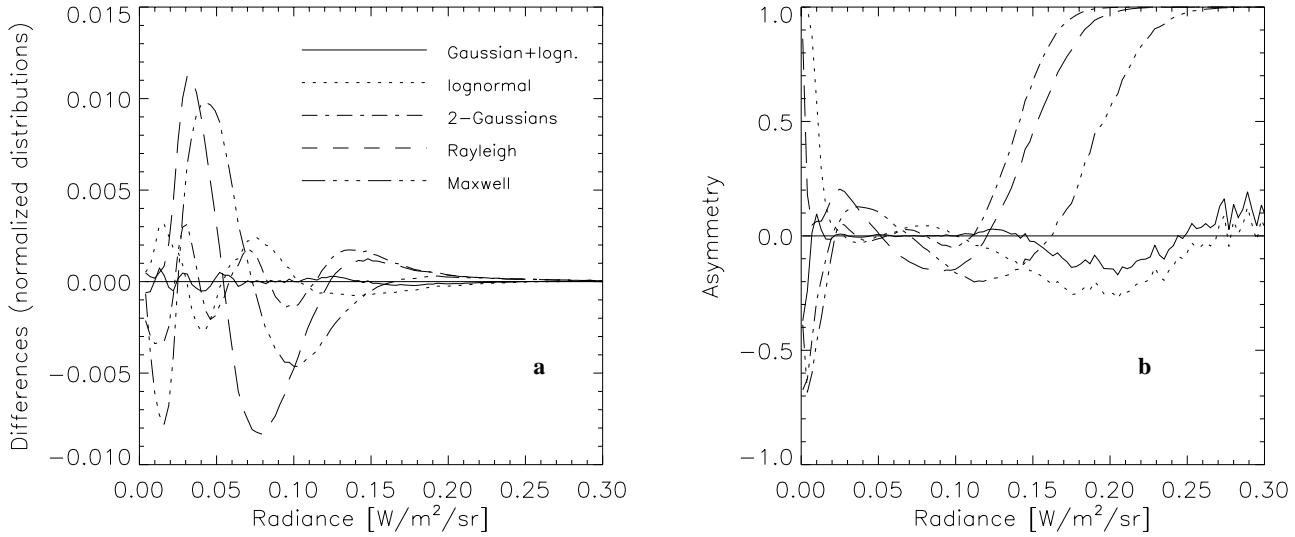
Fig. 5a and b. Example of a graphical representation of the errors of the fits for the various model distributions. Shown are the absolute differences of the (normalized) fit-functions to the (normalized) radiance distribution measured by SUMER at 770 Å **a**, and the relative difference, or asymmetry, of fit and data, i.e. the differences divided by the sum **b**.
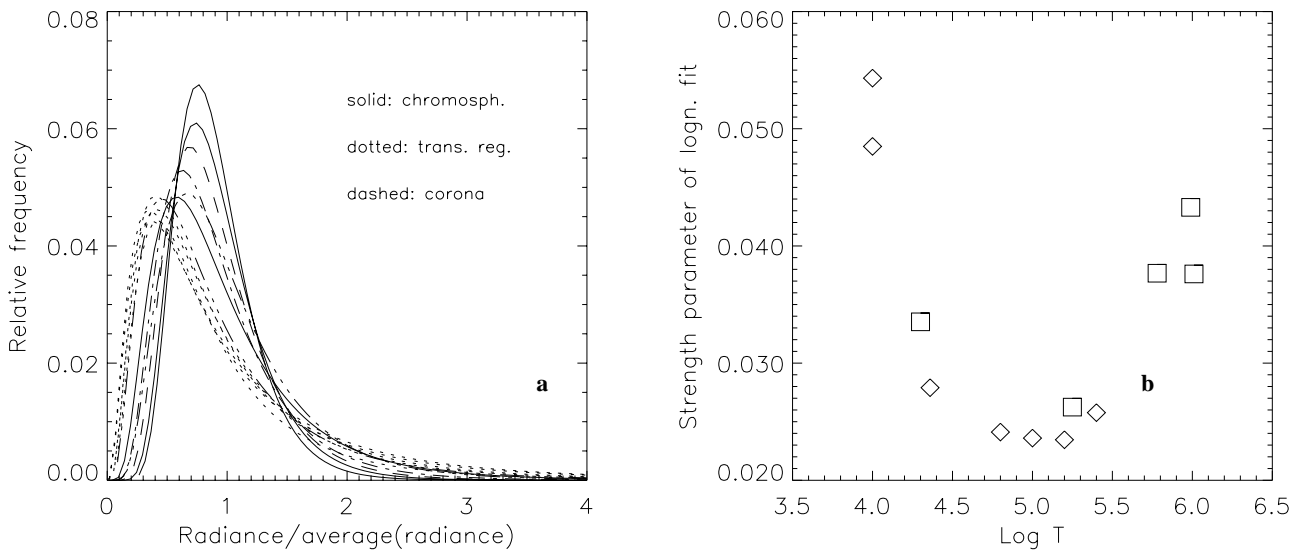
Fig. 6a and b. Lognormal fits to the normalized histograms of SUMER data at different temperatures. Plot **a** shows the fitted functions, plot **b** shows the corresponding strength parameter N_0 of the lognormal fit, which is a measure of the height and position of the peak. The squares represent the results from the larger data sets, the diamonds those of the additional data.

an observed intensity distribution into cell and network parts, fails to give an adequate representation of the long tail of particularly bright pixels. In the few cases in which a double Gaussian distribution provides a better representation of the data (CDS observations of the Mg X lines) we could show that this is the result of the lower spatial resolution of the instrument.

Is a lognormal distribution alone sufficient to describe the intensity distributions of all lines, or is another component, e.g. a Gaussian, needed? The improved fits to some lines by a lognormal+Gaussian combination speak for the latter. However, the highly variable relative strengths and locations of the two components are a major drawback. Also, a further improvement in the spatial resolution may lead to distributions closer to

a pure lognormal, as an extrapolation from our result suggests. Note that at least at coronal temperatures the intensity distributions are not self-similar in the sense that their shapes depend on the spatial resolution of the observations. This confirms that the relevant scales of coronal heating lie at or below the spatial resolution of SUMER.

The fact that in most cases the lognormal distribution is to be preferred to a double Gaussian provides support for the idea that basically the same heating processes are acting in the network and cell interiors. Whether it also supports the conclusion of Griffiths et al. (1999) that small-scale magnetic fragmentation processes could be responsible for the observed radiances also at chromospheric and transition region temperatures is far less
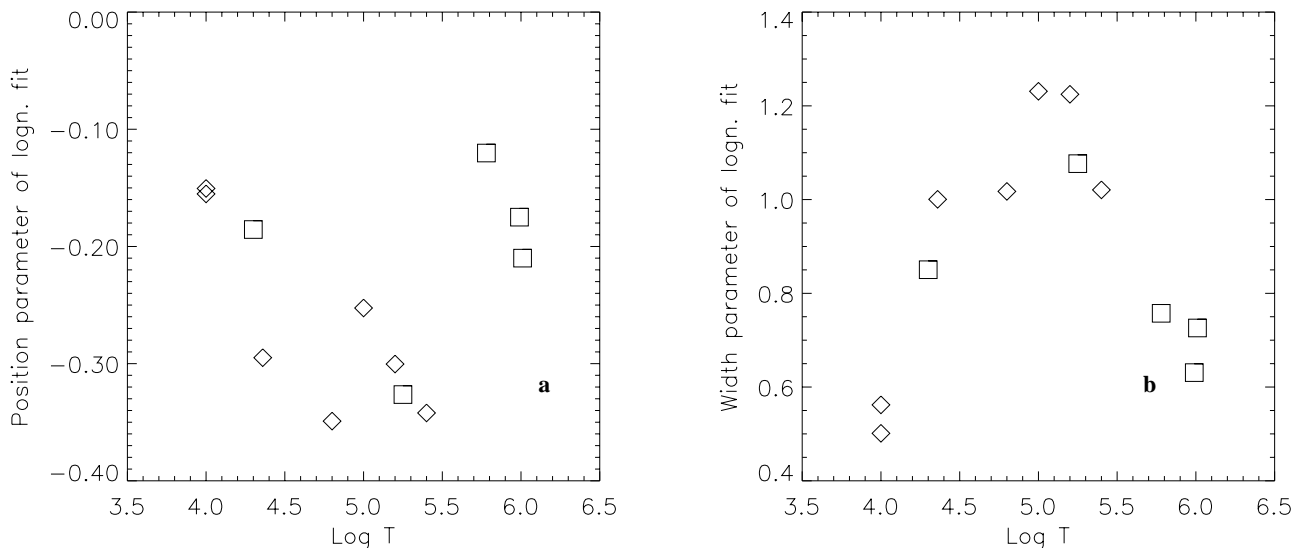
Fig. 7a and b. The other two fit parameters corresponding to Fig. 6. (Note that due to the normalization the three parameters are not independent.) Plot **a** shows the position parameter μ, plot **b** shows the width parameter σ of the lognormal fit.

clear. They base their conclusion on the work of Bogdan et al. (1988), who studied the size distribution of sunspot umbrae and found it to be lognormally distributed. They (Bogdan et al. 1988) pointed out that the lognormal distribution is an indicator of fragmentation processes (Kolmogorov 1941), in the sense that, starting from an initial quantity A_0, after n fragmentations into fractions x_i and $(1 - x_i)$ the stochastic quantity A_n is given as a product of independent variables, $A_n = A_0 \Pi_{i=0}^{n}(1 - x_i)$. The Central Limit Theorem then applies for the logarithm of A_n if the x_i are independent, have the same probability distribution, and their logarithm has finite variance. Thus, this logarithm is normally (Gaussian) distributed.

Lognormal distributions are not unknown in solar and astrophysics. Early studies showed that the distribution of galaxies could be described with a lognormal function (Hubble 1934; Szalay 1987). While Bogdan et al. (1988) used the lognormal distribution to model the distribution of sunspot umbral areas, Martínez Pillet et al. (1993) found sunspot decay rates to be lognormally distributed.

In the case of sunspot umbrae the connection with magnetic fragmentation processes is straightforward. Sunspots represent cross-sections through magnetic flux-tubes. A lognormal distribution of umbral areas thus implies that the flux tubes crossing the solar surface have undergone (or are undergoing) fragmentation. Since the field strength averaged over the cross-section is practically independent of its area (Solanki & Schmidt 1993; Solanki et al. 1999) sunspot umbral area is also rather tightly related to the magnetic flux carried by the flux tube. According to current understanding sunspots and the smaller flux tubes forming pores or underlying plages were part of a single large tube at the bottom of the convection zone. While rising through the convection zone this tube, which carried the flux of the entire active region, was shredded near its apex (Zwaan 1985), thus giving rise to the expectation of a lognormal distribution of the resulting flux tube cross-sections.

The EUV brightenings visible from the chromosphere to the corona are also related to the magnetic field, but far less directly. E.g. Schrijver et al. (1989) found that the relationship between chromospheric brightness and photospheric magnetic field exhibits a huge scatter and is thus far from being one-to-one. Theoretically, the mere presence of a magnetic field is not sufficient to result in an EUV brightening. Rather, the brightness seen in EUV lines is produced by the cooling of gas previously heated up through some dynamic process involving the magnetic field. This may be the dissipation of MHD waves or the release of magnetic tension energy, built up through footpoint motions, by magnetic reconnection. It is thus unclear to what extent the lognormal distribution of EUV brightnesses reflects the lognormal distribution of the magnetic fluxes in the tubes and to what extent it is produced by the statistics of the physical processes generating the brightness. Thus it would be interesting to work out the brightness distribution predicted by the sandpile model of Lu & Hamilton (1991), which predicts a power law distribution of the brightenings. Also of considerable interest would be to follow the change in the shape of the distribution from coronal holes, via the quiet Sun to active regions. We plan to follow up both these paths in future investigations.

References

Athay R.G., 1982, ApJ 263, 982

Bocchialini K., Vial J.-C., Einaudi G., 1997, Proc. of the 5th SOHO Workshop, Oslo, Norway, ESA SP-404, 211

Bogdan T.J., Gilman P.A., Lerche I., Howard R., 1988, ApJ 327, 451

Dammasch I.E., Hassler D.M., Curdt W., Wilhelm K., 1999, Space Sci. Rev. 87, 161

Dowdy J.F. Jr., Rabin D., Moore R.L., 1986, Sol. Phys. 105, 35

Gabriel A.H., 1976, Phil. Trans. R. Soc. London, Ser. A 281, 339

Gallagher P.T., Phillips K.J.H., Harra-Murnion L.K., Keenan F.P., 1998, A&A 335, 733

Griffiths N.W., Fisher G.H., Woods D.T., Siegmund O.H.W., 1999, ApJ 512, 992

Harrison R.A., Sawyer E.C., Carter M.K., et al., 1995, Sol. Phys. 162, 233

Haugan S.V.H., 1999, Sol. Phys. 178/2, 275

Hubble E., 1934, ApJ 79, 8

Huber M.C.E., Foukal P., Noyes R.W. et al., 1974, ApJ 194, L115

Kolmogorov A.N., 1941, C. R. Acad. Sci. USSR 31, 99

Leighton R.B., 1959, ApJ 130, 366

Lemaire P., Wilhelm K., Curdt W., et al., 1997, Sol. Phys. 170/1, 105

Lu E.T., Hamilton R.J., 1991, ApJ 380, L89

Martin S.F., 1988, Sol. Phys. 117, 243

Martínez Pillet V., Moreno-Insertis F., Vázquez M., 1993, A&A 274, 521

Pauluhn A., Rüedi I., Solanki S.K., et al., 1999, Appl. Opt. 38, No. 34, 7035

Reeves E.M., 1976, Sol. Phys. 46, 53

Reeves E.M., Vernazza J.E., Withbroe G.L., 1976, Phil. Trans. R. Soc. London, Ser. A 281, 319

Schrijver C.J., Coté J., Zwaan C., Saar S.H., 1989, ApJ 337, 964

Solanki S.K., Steiner O., 1990, A&A 234, 519

Solanki S.K., Schmidt H.U., 1993, A&A 267, 287

Solanki S.K., Finsterle W., Rüedi I., Livingston W., 1999, A&A 347, L27

Szalay A., 1987, In: Martinet L., Mayor M. (eds.) 17th Advanced Course of the SSAA, Observatoire de Genève, Switzerland, p. 175

Teriaca L., Banerjee D., Doyle J.G., 1999, A&A 349, 636

Thompson W.T., 1998, CDS Software Note 49, http://orpheus.nascom.nasa.gov/cds/software_notes.html

Thompson W.T., Brekke P., 1999, submitted to Sol. Phys.

Wilhelm K., Curdt W., Marsch E., et al., 1995, Sol. Phys. 162, 685

Zwaan C., 1985, Sol. Phys. 100, 397